Validation of the IRI 2016 and IRI-Plas 2017 models over central Asian mid-latitude regions in the descending phase of solar cycle 24

Yekoye Asmare Tariku

Department of Space Science and Research Applications Development, Institute of Ethiopian Space Science and Technology, Addis Ababa, Ethiopia

* Corresponding author. Tel. +251912799754

Email_address:yekoye2002@gmail.com (Yekoye Asmare)

Abstract

This paper investigates the performance of the latest versions of the IRI model (IRI 2016 with NeQuick, IRI01-corr and IRI2001 options for the topside electron density) and the IRI extended to the plasmasphere (IRI-Plas 2017) models in the estimation of the Vertical TEC (VTEC) variation over the central Asian mid-latitude regions in the descending phase of solar cycle 24 (2014-2016). The GPS dual frequency receivers installed at Kurchatov, KRTV (geog 50.71°N, 78.62°E, Geom. 41.84°N), Khantau, SUMK (44.21°N, 74.00°E, Geom. 35.73°N), Talas, TALA (42.45°N, 72.21°E, Geom.34.13°N) and Kazarman, KAZA (41.38°N, 73.94°E, Geom.32.92°N) have been used to derive the estimate of the vertical TEC (GPS-VTEC) for the comparison of the monthly and seasonal performance of the models. The modelled VTEC values generally tend to be larger than the GPS-VTEC values during periods of high solar irradiance (daytime hours), with the highest overestimation being observed by IRI-Plas 2017 model followed by IRI 2016 model with the IRI2001 topside option. However, the differences between the models and

between the models and the GPS-VTEC values become diminished as the solar irradiance decreases, with the highest underestimation being observed by the IRI 2016 model with NeQuick topside option. It has also been shown that the smallest root-mean-square deviations between the GPS-VTEC and modelled VTEC are observed generally in the June solstice months, showing that the models perform best during local summer. On the contrary, the largest root-mean-square deviations between the modelled VTEC and GPS-VTEC are observed during high solar irradiance on the surface of the Earth (especially in the time interval between 05:00 and 10:00 UT which corresponds to the daytime hours 10:00 and 15:00 LT), showing that the models perform poorly during high solar irradiance. In addition, both the IRI 2016 and IRI-Plas 2017 models show a progressive decline in VTEC during a negative storm, but do not adequately estimate the storm time VTEC variation.

Key words: GPS TEC; IRI 2016 TEC; IRI-Plas 2017; mid-latitude Asian TEC

1. Introduction

The ionosphere is the upper region of atmosphere of the Earth that is ionized by cosmic and solar radiation. Because of the refracting and reflecting nature of the ionosphere, the radio wave propagations through it are strongly affected **(Matsushita and Campbell, 1967).** Hence, the operation of the various satellite communications, navigation, positioning systems (such as the Global Positioning System, GPS) greatly relies on the state of the ionosphere in relation to the electron distribution. When signals are transmitted from the GPS satellite to the receivers on the ground through the ionosphere, the free electrons between the receiver and the satellite orbit at a height of about 20,200 km called the Slant Total Electron Content (STEC) largely influence the

transmission of the signals, resulting in delay for the signal arrival time at the receivers' position (Ioannides and Strangeways, 2000). According to Bradford and Spilker (1996), this could result in range-rate errors for the GPS satellites users with high accuracy measurements.

Even though it was originally developed for military purposes, the GPS has also been used for different applications. One of the uses of the GPS for researchers is to measure the TEC in different ionospheric regions. For the measurement of TEC, dual frequency receivers are more advantageous than the single frequency receivers. This is because the dual frequency receivers are better to minimize ionospheric errors and provide integral information about the ionosphere as compared to that of the single frequency receivers (Klobuchar et al., 1996; Mannucci et al., 1998; Ciraolo et al., 2007; Nahavandchi and Soltanpour, 2008). Such TEC extracted from the dual frequency GPS receivers are called GPS derived-VTEC (GPS-VTEC). In addition, it is necessary to convert the slant TEC (STEC) into the equivalent vertical TEC (VTEC) at a mean ionospheric height of about 300 km to better characterize the TEC over a given receiver position and see the overall ionization of the Earth's ionosphere.

However, on some occasions where the GPS-TEC data are not available, it is common to rely on empirical models, such as the International Reference Ionosphere (IRI) and the IRI extended to the plasmasphere (IRI-Plas). The IRI model has been used to provide monthly median values of TEC. To improve its performance, the model has been updated many times employing worldwide ground and space based data (Bilitza, 2003). As a result, by incorporating some new input parameters that can empower its performance, a new version of the model (IRI 2016) has been released in 2017. Similar to the previous versions of the model, the IRI 2016 model provides the monthly averages of TEC in the altitude range of about 50 to 2000 km (Bilitza et al., 2017). The possibility of the IRI model for all released versions (including IRI

2016) to estimate the TEC is limited only up to an altitude of 2000 km; while, the TEC obtained from GPS receivers includes free electrons up to the GPS orbit altitude of 20200 km. This makes it challenging to comprehensively assess the performance of the IRI model for TEC estimation using the TEC inferred from the GPS receivers. To resolve this problem, the IRI-Plas model (the IRI extended to the plasmasphere) which can estimate the TEC variation up to a height of 20,200 km has been proposed (Gulyaeva et al., 2002; Gulyaeva and Bilitza, 2012). Like that of the IRI model, the IRI-Plas model has been updated and reached the most recent version (IRI-Plas 2017) in 2018. It is also used to obtain the monthly mean values of different ionospheric parameters (such as TEC) up to an altitude of 20200 km (Sezen et al., 2018).

Different findings (such as McNamara, 1985; Abdu et al., 1996; Scida et al., 2012; Asmare, et al., 2014; Ezquer et al., 2014) reported that the IRI model does not show good performance over the equatorial and low latitude regions. Ezquer et al. (2014), for instance, showed that large deviations are observed between the GPS-VTEC and modelled (IRI 2012) foF2 values over the southern crest of the equatorial anomaly in the American region during the period 2008-2009. On the other hand, many researchers **(e.g.** Bilitza et al., 1990; Dai and Ma, 1994; Bhuyan and Borah, 2007; Akala et al., 2013; Luo et al., 2014; Li et al., 2016) reported that the estimation of the TEC values by the IRI model is good in the mid-latitude regions. For instance, Dai and Ma (1994) conducted research on the IRI-86 and IRI-90 models' performance over Asian mid latitude regions and found that both versions of the IRI model generate acceptable values of TEC which are comparable to TEC derived from Faraday rotation during low solar activity. They found that IRI-90 performed better than IRI-86. Luo et al. (2014) also tried to evaluate the performance the IRI 2012 model in the low and mid-latitude regions of China during the moderate solar activity. They noted that the IRI 2012 model performs better in the mid-latitude regions than in the low-

latitude regions. In addition, Li et al. (2016) also showed the IRI 2012 model underestimates the lowest TEC values in all months over China. They also explained that the TEC values throughout the day were underestimated by the model in the June solstice months in 2009 and 2013. Zakharenkova et al. (2015), Adebiyi et al. (2016) and Ezquer et al. (2017) also showed that the IRI-Plas model overestimates the TEC values obtained from GNSS receivers during the daytime hours. According to Ezquer et al. (2017) the inaccurate estimation of the plasmaspheric TEC could be one of the reasons for the overestimation of TEC by the IRI-Plas model. Okoh et al. (2018), employing the IRI-Plas 2017 model, also showed that the IRI-Plas overestimates the GNSS-derived TEC values mostly during the local daytime hours over all longitude sectors including the Asian sector.

As shown above, most of the comparisons of the performance of the empirical models were done employing the old versions of the models. Moreover, simultaneous validation of the recent versions of the models (IRI 2016 and IRI-Plas 2017) with ground based measurements at different regions have been lacking during long lasting solar activity periods. Hence, in spite of good opportunities in testing the improvements of the models, adequate studies have not yet been conducted to compare the performance of the recent version of the two models in TEC estimation in the descending phase of solar cycle 24 (2014-2016) over the central Asian mid latitude regions. On the other hand, testing the performance of the models is important in order to select and use them for the estimation of VTEC on occasions and at locations when GNSS derived VTEC data are not available**.** Hence, this work extensively evaluates the performance of the IRI 2016 model with the three topside options for the electron density (NeQuick, IRI01-corr and IRI2001) and IRI-Plas 2017 model for the estimation of TEC variation over the region. The study addresses the limitations of the models and reports its findings to the scientific community

in general and the empirical modellers in particular in order to facilitate the improvement of the performance of the models in the estimation of VTEC over the central Asian mid latitude. The results from this study are also important to recommend the best model for the estimation of the VTEC variation over the central mid latitude Asian regions in descending phase of solar cycle 24.

2. Data and method of analysis

The dual frequency GPS receivers installed at different central mid latitude Asian regions: Kurchatov, KRTV (geog 50.71°N, 78.62°E, Geom. 41.84°N), Khantau, SUMK (44.21°N, 74.00°E, Geom. 35.73°N), Talas, TALA (42.45°N, 72.21°E, Geom.34.13°N) and Kazarman, KAZA (41.38°N, 73.94°E, Geom.32.92°N) have been considered to get the required TEC data for the study during the descending phase of solar cycle 24 (2014-2016). The locations of the GPS receivers used for the study are given in Figure 1. The selection of the stations was based on the availability of a complete record of GPS data from these receivers during the years of interest. Since the GPS TEC data obtained from UNAVCO website (http://facility.unavco.org/data/dai2/app/dai2.html) were recorded in the Receiver Independent Exchange Format (RINEX), the Gopi Seemala software version 2.9.5 has been used to process and convert to the observed TEC data (Seemala, 2017). The conversion of STEC to VTEC was done using a thin shell model with an assumed ionospheric altitude of 300 km, and only TEC data recorded for ray paths with elevations greater than 30º were considered to minimize the errors due to multipath effects. **The altitude of 300 km used for the thin shell model is coded in the software used for the derivation of GPS TEC. This altitude is within the range of the peak density of the F2 layer, h_m, which Norsuzila et al. (2008) claimed to usually range from 250 to 350 km at mid-latitudes. In this study, the ionospheric pierce**

points (IPP) have been assumed to occur at the height of maximum electron density, h_m=300 km. The latest version of the IRI model (IRI 2016) with the three options for the topside electron density (NeQuick, IRI01-corr and IRI2001) has been used for the IRI modelled TEC data. In addition, the Gul-1987 for bottomside thickness and the CCIR option for the F2 peak density have been used (see the model web site, https://ccmc.gsfc.nasa.gov/modelweb/models/iri2016_vitmo.php). In the same way, the corresponding IRI-Plas model TEC values have been obtained from the latest version of the model (IRI-Plas 2017). Like that of the IRI 2016 model, the Gul-1987 option for the bottomside thickness and CCIR for F-peak option have been used (see **http://www.ionolab.org/iriplasonline/**). Here, because the study is conducted over the continent, the CCIR option has been used for both models.

In order to evaluate the performance of the models in terms of the monthly means of diurnal variations, the mean diurnal hourly VTEC values of magnetically quiet days in each month were determined during the period 2014-2016**.** The magnetically quiet days are those whose **Dst>-30 nT**. Similarly, to investigate the seasonal VTEC variations while validating the models, the diurnal mean hourly VTEC values were averaged over each season. The seasons were classified as September equinox (August, September and October), December solstice (November, December and January), March equinox (February, March and April) and June solstice (May, June and July). The root-mean-square deviations between the GPS-VTEC and modelled VTEC values have been also computed to better evaluate the diurnal VTEC prediction performance of the models. Similarly, the percentage differences between each of the experimental monthly and seasonal hourly mean VTEC values and the corresponding modelled VTEC values have been

computed. The computation has been done by subtracting the GPS VTEC values from the corresponding IRI 2016 and IRI-Plas 2017 VTEC values.

3. Results and discussion

3.1 Diurnal monthly and seasonal performance evaluation of the IRI 2016 and IRI-Plas 2017 models

Figures 2-11 show the monthly and seasonal diurnal VTEC variations and performance of the IRI 2016 and IRI-Plas 2017 models. The results show that the mean and maximum values of both the GPS-VTEC and modelled VTEC decrease from 2014 to 2016. For instance, the highest peak GPS VTEC values of about 50 TECU being observed in March during 2014 reduces to about 35 and 20 TECU in 2015 and 2016, respectively over Kurchatov station in the same month. Similarly the highest peak IRI 2016 (with NeQuick option) and IRI-Plas 2017 VTEC values of about 65 and 80 TECU being observed during 2014 in April decreases to 60 and 70 TECU, respectively in 2015 and 20 and 25 TECU, respectively during 2016 in the same month (see Figs. 2-7). Similarly, the highest GPS, IRI 2016 (with NeQuick option) and IRI-Plas 2017 seasonal VTEC values of about 30, 55 and 75 TECU, respectively being observed in the March equinox during 2014 decreases to about 30, 35 and 50, respectively in 2015 and 20, 21 and 25, respectively in 2016 in the same season (see Figs. 8-11). Moreover, both the GPS-VTEC and modelled VTEC show the lowest diurnal hourly values at 00:00 UT (05:00 LT), as expected, since the Seemala GPS-TEC software adjusts the receiver biases so that the VTEC from all observed satellites coincide at 05:00 LT and are equal to the lowest values for the day (see Figs. 2-7). This gradual increment of the VTEC in the daytime hours to reach the peak value at the noontime hours is due to the diurnal variation of solar EUV (Ezquer et al., 2014). Since the peak

VTEC is linked to the solar zenith angle, the peak VTEC values increase with the EUV peaks at local noon time hours (Balan et al., 1994). Moreover, as shown in the Figures (see Figs. 2-11), the modelled VTEC for both the IRI 2016 and IRI-Plas 2017 VTEC values are generally larger than the GPS-VTEC, especially when the solar zenith angle increases, with the highest values being observed by the IRI-Plas 2017 followed by the IRI 2016 model with IRI2001 option. However, as the solar zenith angle decreases, the modelled VTEC generally have values closer to the GPS-VTEC values, especially in the June solstice months. As shown in Figs. 2-11, the highest monthly and seasonal root-mean-square deviations (due to overestimation of VTEC by the IRI-Plas 2017 model) of about 2.5 and 1.5 are observed in April and during the March equinox, respectively over Kurchatov in 2014, showing that the performance of the model is relatively poor during the local daytime, mostly in the time interval between 05:00 and 10:00 UT (10:00-15:00 LT).The IRI 2016 model with NeQuick and IRI2001 topside options show high root-mean-square deviations after the IRI-Plas 2017 model which showed the highest deviation, proving that the IRI 2016 model with those topside options has poor performance, especially in the described time interval. On the other hand, the lowest root-mean-square deviations are observed during night-time when the solar activity decrease for both the IRI 2016 and IRI-Plas 2017 models showing that the performance of the models improve as the solar activity decreases from 2014 to 2016.

Other researches related to the IRI 2016 and IRI-Plas 2017 models' TEC estimation performance showed similar results proving that both models mostly underestimate the TEC values in the low solar activity phase. For example a research conducted over China regions by Li et al. (2016) showed that the IRI 2012 model underestimates the lowest TEC values in all months. They also explained that the TEC values throughout the day were underestimated by the

model in the June solstice months in 2009 and 2013. The limited performance of the IRI model may be resulting from poor estimation performance of the hmF2 and foF2, as noted by Chakraborty et al., 2014, Kumar et al, 2015. Zakharenkova et al. (2015), Adebiyi et al. (2016) and Ezquer et al. (2017) also showed that the IRI-Plas model overestimates TEC observations obtained from GNSS receivers during the daytime hours. Zakharenkova et al. (2015), for instance, conducted a study to identify the cause for the discrepancy observed between the modelled and measured TEC; they found that both the IRI and IRI-Plas models do not correctly represent the topside electron density profile, leading to overestimation of the electron density of the F2 peak. They noted that the main source for the discrepancy is not the plasmaspheric TEC; rather the problem is the poor IRI topside ionosphere representation. Hence, further investigations have to be made to resolve the limitation of the models for the topside ionosphere representation.

3.2 Monthly and seasonal mean performance evaluation of the IRI 2016 and IRI-Plas 2017 models

Figs. 12 and 13 show the monthly and seasonal mean VTEC variations and prediction performance of the models. Both the GPS-VTEC and the modelled VTEC are observed to have peaks in the equinoctial months in 2014 when the solar activity was the highest during the three-year period of observation. For more information see http://www.sidc.be/sunspot-data/. In 2016 when the solar activity is at the lowest value during the period of observation, the highest GPS-VTEC values are observed in the June solstice months. However, none of the models have the same trend. They all show decreasing mean VTEC values from winter solstice to summer solstice (Figure 12). For instance, the highest monthly GPS, IRI 2016 (with NeQuick option) and

IRI-Plas 2017 VTEC values of about 28, 40 and 51 TECU, respectively being observed in observed in 2014 during March (for GPS-VTEC) and April (for modelled VTEC) diminish in 2015 to highest values of about 20, 37 and 48 TECU, respectively in April (for both GPS-VTEC and modelled VTEC) and in 2016 to 18, 10 and 15 TECU, respectively in May (for GPS_VTEC) and April (for modelled VTEC) (see the top panels of Figure 12). Overestimations (with the highest being observed in using IRI-Plas 2017 model followed by IRI 2016 model with NeQuick option) are mostly observed during 2014 when the solar activity was the highest during the period of observation. Underestimations (with the worst being observed by the IRI 2016 model with NeQuick option) are mostly observed during 2016 when the solar activity decreased to the minimum during the period of observation (see the bottom panels of Figure 12 and 13). The highest monthly overestimations of about 65% by IRI-Plas 2017 model and 55% by the IRI 2016 model with NeQuick option was observed in April 2014. The overestimations decreased to about 60% and 40%, respectively in the same month in 2015. However, in 2016, the year with the lowest solar activity during the period of observation, overestimation of about 25% is only observed in the IRI-Plas 2017 model in April, but the IRI 2016 model with all the three options tends to underestimate the GPS-VTEC values in April, while all the models have a significant underestimation of GPS-VTEC in May. The highest monthly underestimation during the period 2014-2016 was the underestimation of about 95% observed in May 2016 for the IRI 2016 model with NeQuick option (see the bottom panels of Figure 12). Similarly, the highest seasonal overestimation of about 60% is observed in the December solstice in 2015; while, the highest underestimation of about 90% is observed in the June solstice in 2016. Overall, using the IRI 2016 model with the IRI01 topside option shows the best performance of all the models during the highest solar activity during 2014-2016. On the other hand, when the solar activity was the

lowest the IRI 2016 model with the IRI2001 topside option and IRI-Plas 2017 showed better performance than the other models

3.3 Response of the IRI 2016 and IRI-Plas 2017 models during storm time TEC variation

To study storm time performance of the models, the storm-time options in the IRI 2016 model with NeQuick, IRI01 and IRI2001 options for the topside electron density and IRI-Plas 2017 model versions have been switched on and the GPS VTEC observed over KRTV station was compared to the corresponding IRI 2016 and IRI-Plas 2017 VTEC on a magnetic storm day (with a peak Dst index of about -204 nT on 2015-06-23). As shown in Figure 14, the storm started on 2015-06-22 at about 15:00 UT (07:00 LT) and the recovery phase of the storm is observed on. 2015-06-24**.** Hence, the patterns of the VTEC fluctuations during the initial phase (2015-06-22) and the recovery phase (2015-06-24) of the storm were also considered to better see the effect of the storm on the VTEC. As shown in Figure 15**,** the sharp decrease of the GPS VTEC shows that the occurrence of a storm was observed. On the other hand, the IRI 2016 and IRI-Plas 2017 VTEC values show limited fluctuations when the storm models are "on" (see Figs.15a-15c and Figs.15d-15f) and were not able to respond to the sharp decrease in TEC seen in the GPS VTEC values. As shown in the figure, the modelled VTEC variations follow almost similar pattern in all the three days; they generally tend to underestimate the VTEC values and do not able to respond to the sharp increase or decrease of the GPS VTEC values. The modelled VTEC values for both models tend to be larger than those of the GPS-VTEC values, especially in the main phase of the storm when the storm option is 'off'. However, when the storm option is 'on', the modelled values tend to be smaller than the corresponding GPS-VTEC values. But, both generally show a decrease in TEC during the main phase of the storm and an increase during the recovery phase of the storm. According to the 2015 St. Patrick's Day storm, short

period of strong disturbances resulting from sub storms which can release energy and particles that were left in the magnetosphere after the main event may result in the enhancement of TEC in the recovery phase of the storm (Stanley and Linnea, 2016). In general, the overall results show that, although both models fail to respond to the sharp decrease of the TEC as seen in the GPS VTEC during the storm, the IRI-Plas 2017 model is better in estimating the storm time VTEC variations, followed by the IRI 2016 model with IRI2001option. Therefore, it is important to minimize the limitation of the models and further improve their performance in the estimation of the ionospheric variability of TEC during storm time condition.

4. Conclusions

.This paper discusses the performance evaluation of the IRI 2016 model with the three options for the topside electron density (NeQuick, IRI01-corr and IRI2001) and the IRI-Plas 2017 model for monthly and seasonal TEC estimation employing the GPS TEC data obtained from the dual frequency receivers located at the central mid-latitude Asian regions during the period 2014-2016. It has been observed that the variability of the diurnal VTEC values show minima at about 00:00 UT or 05:00 LT and maxima mostly in the time interval between 05:00 and 10:00 UT (10:00–15:00 LT). As expected, the minimum and maximum monthly mean hourly VTEC values are observed in the solstice and equinoctial months, respectively when the solar activity is high; however, when the solar activity is low (especially in 2016) the maximum VTEC values shift to the June solstice months. It has also been shown that both the IRI 2016 and IRI-Plas 2017 models tend to generally overestimate the VTEC variations, especially when the solar activity is highest, with the highest overestimation being observed by the IRI-Plas 2017 model, followed by the IRI 2016 model with IRI2001 option. On the other hand, the highest underestimations are mostly

observed when the solar activity is lowest, with the worst underestimation being observed by the IRI 2016 model with the NeQuick option. However, both models show low root-mean-square deviations during local nighttime (especially in the June solstice) during both the low and high solar activities, with the IRI 2016 model with NeQick and IRI0-corr showing generally the best performance. On the contrary, relatively high root-mean-square deviations (mainly due to overestimation of VTEC) are observed mostly in the local daytime between 05:00 and 10:00 UT (10:00-15:00 LT) by both the IRI 2016 and IRI-Plas 2017 models, with the IRI-Plas 2017 model showing the worst performance. Moreover, both the IRI 2016 and IRI-Plas 2017 models do not adequately respond to the sharp increase or decrease of the GPS VTEC variation during storm time condition. Hence, further improvements have to be made to enhance the models' performance in TEC estimation over the central mid-latitude Asian regions.

Acknowledgements

The data of daily sunspot number, GPS and IRI model for this paper are freely available at: http://www.sidc.be/sunspot-data/, http://facility.unavco.org/data/dai2/app/dai2.html and **http://IRImodel.org,** respectively. Hence, the author is very thankful to NOAA, UNAVCO, and NASA for providing free daily sunspot number, GPS and online IRI model, respectively. The author is also very thankful to IONOLAB and Dr Gopi Seemala for providing free online IRI-Plas data (http://www.ionolab.org/iriplasonline/) and GPS-TEC software used for the calculation of GPS-VTEC, respectively in this paper.

References

Adebiyi SJ, Adimula I.A, Oladipo OA, Joshua BW (2016). Assessment of IRI and IRIPlas models over the African equatorial and low-latitude region. J. Geophys. Res. 121, 7287–

7300. https://doi.org/10.1002/2016JA022697

Akala A O, Seemala JK, Doherty PH, Valladares CS, Carrano CS, Espinoza J, Oluyo S (2013). Comparison of equatorial GPS-TEC observations over an African station and an American station during the minimum and ascending phases of solar cycle 24, Ann. Geophys., 31, 2085–2096, doi:10.5194/angeo-31-2085

Balan, N, G. J. Bailey, B. Jenkins, P. B. Rao, R. J. Moffett (1994). Variations of ionospheric ionization and related solar fluxes during an intense solar cycle, Journal of Geophysical Research: Space physics, 99(2), 2243-2253

Bilitza D M, Hernandez-Pajares J M. Juan, Sanz J (1990). Comparison between IRI and GPS-IGS derived electron content during 1991-97, *Phys. Chem. Earth* 24C (4), 311–319.

Bilitza D. (2003). International Reference Ionosphere 2000: Examples of improvements and new features. Adv. Space Res. 31, 151–167.

Bilitza D, Altadill D, Truhlik V, Shubin V, Galkin I, Reinisch B, Huang X (2017). International Reference Ionosphere 2016: from ionospheric climate to real-time weather predictions, Space Weather, DOI: 10.1002/2016SW001593.

Bradford WP, Spilker JJ (1996). Global Positioning System: Theory and applications, American Institute of Aeronautics and Astronautics, Vol. I and II Washington DC, USA.

Chakraborty M, Kumar S, Kumar B, Guha A (2014). Latitudinal characteristics of GPS derived ionospheric TEC. a comparative study with IRI 2012 model, Annals of Geophysics, 57 (5), A0539; doi: 10.4401/ag-6438.

Ciraolo L, Azpilicueta F, Brunini C, Meza A, Radicella S M (2007). Calibration errors on experimental slant total electron content (TEC) determined with GPS, *J., Geodesy*, 81,

111–120.

Dai K, Ma J (1994) Comparison of total electron content calculated using the IRI with observations in China, *J. Atmos. Sol. Terr. Phys.* 56, 3, 417-422, DOI: 10.1016/0021-9169(94)90222-4.

Ezquer RG., López J L , Scidá L.A, Cabrera MA, Zolesi, B , Bianchi C Pezzopane M, Zuccheretti E, Mosert M (2014), Behaviour of ionospheric magnitudes of F2 region over Tucumán during a deep solar minimum and comparison with the IRI 2012 model predictions, Journal of Atmospheric and Solar-Terrestrial Physics, 107, 89–98

Ezquer RG, Scida LA, Orue Y M, Nava B, Cabrera M A, Brunini C (2017). NeQuick 2 and IRI Plas VTEC predictions for low latitude and South American sector. Adv. in Space Res. https://doi.org/10.1016/j.asr.2017.10.003.

Gulyaeva T.L, Huang X, Reinisch BW (2002). Plasmaspheric extension of topside electron density profiles. Adv. Space Res. 29 (6), 825–831

Gulyaeva T L, Bilitza D (2012). Towards ISO Standard Earth Ionosphere and Plasmasphere Model, in New Developments in the Standard Model, edited by R. J. Larsen, pp. 1–39, Nova, Hauppauge, New York.

Gulyaeva, T.L., Arikan, F., Sezen, U. and Poustovalova, L.V., (2018). Eight proxy indices of solar activity for the International Reference Ionosphere and Plasmasphere model. Journal of Atmospheric and Solar-Terrestrial Physics, *172*, pp.122-128.

Ioannides RT, Strangeways HJ (2000). Ionosphere-induced errors in GPS range finding using MQP modelling, ray-tracing and nelder-mead optimization, Millennium Conference on Antennas and Propagation, AP2000, vol. II, Davos, pp. 404–408, Switzerland

Kumar S, Tan E, Murti D (2015). Impacts of solar activity on performance of the IRI-2012 model predictions from low to mid latitudes. Earth, Planets, Space, 67:42. doi:10.1186/s40623-015-0205-3

Klobuchar J A, Parkinson BW, Spilker J.J (1996). Ionospheric effects on GPS, in Global Positioning System: theory and applications, American Institute of Aeronautics and Astronautics, Washington D.C.

Li S Lihua L, Junhuan P (2016). Variability of Ionospheric TEC and the Performance of the IRI-2012 Model at the BJFS Station, China, Acta Geophysica, vol. 64 (5) pp. 1970-1987, DOI: 10.1515/acgeo-2016-0075

Luo W, Liu Z, Li M (2014). A preliminary evaluation of the performance of multiple ionospheric models in low- and mid-latitude regions of China in 2010-2011, *GPS Solution.* 18, 2, 297-308, DOI: 10.1007/s10291-013-0330-z.

Mannucci A J, Wilson B D, Yuan D N, Ho C H, Lindqwister U J, Runge T F (1998), A global mapping technique for GPS-derived ionospheric total electron content measurements, Radio Sci., 33, 565–582, doi: 10.1029/97RS02707.

Matsushita, S. and Campbell, W.H. eds., (1967). Physics of Geomagnetic Phenomena: International Geophysics Series (Vol. 1). Academic Press, New York

McNamara, L F (1985). The uses of total electron content measurments to validate emperical models of the ionosphere, Advance in Space Research, 5(7), 81–90.

Nahavandchi H, Soltanpour A (2008). Local ionospheric modeling of GPS code and carrier phase observation, Survey Review, vol. 40,309, 271–284.

Norsuzila Y, Abdullah M, Ismail M (2008) Determination of GPS total electron content using single layer model (SLM) ionospheric mapping function. Int J Comp Sci Net Sec 8(9):154–

169

Okoh, D., Onwuneme, S., Seemala, G., Jin, S., Rabiu, B., Nava, B., Uwamahoro, J. (2018) Assessment of the NeQuick-2 and IRI-Plas 2017 models using global and long-term GNSS measurements, Journal of Atmospheric and Solar-Terrestrial Physics doi: 10.1016/ j.jastp.2018.02.006.

Scidá LA, Ezquer RG, Cabrera MA , Mosert M, Brunini C Buresova D (2012), On the IRI 2007 performance as a TEC predictor for the South American sector, Journal of Atmospheric and Solar-Terrestrial Physics, Vol. 81–82, pp 50–58, doi:10.1016/j.jastp.2012.04.001

Seemala G (2017). GPS-TEC analysis application, Indian Institute of Geomagnetism (IIG), http://seemala.blogspot.com/2017/09/gps-tec-program-ver-295.html.

Sezen U, Gulyaeva TL, Arikan F (2018). Performance of solar proxy options of IRI-Plas model for equinox seasons, Journal of Geophysical Research: Space Physics, 123(2), pp. 1441-1456,. doi:10.1002/2017JA024994

Zakharenkova IE, Cherniak IV, Krankowski A, Shagimuratov II (2015). Vertical TEC representation by IRI 2012 and IRI Plas models for European midlatitudes. Adv. Space Res. 55, 2070–2076. https://doi.org/10.1016/j.asr.2014.07.027.

Figure captions

Figure 1: Location of the stations used for the study

Figure 2: Monthly means of diurnal VTEC variation and validation of the IRI 2016 and IRI-Plas 2017 models over Kurchatov (KRTV) in 2014

Figure 3: Root-mean-square deviation between the monthly means of diurnal GPS-VTEC and

Figure 12: Monthly arithmetic means of diurnal hourly VTEC variation and validation of the IRI 2016 and IRI-Plas 2017 models over Kurchatov (KRTV) during 2014-2016

Figure 13: Seasonal arithmetic means of diurnal hourly VTEC variation and validation of the IRI 2016 and IRI-Plas 2017 models over Kurchatov (KRTV) during 2014-2016

Figure 14: Dst index on 2015-06-22 to 2015-06-24 (data source for Dst index: World Data Center, Kyoto University).

Figure 15. Variation of the VTEC and response of the IRI 2016 and IRI-Plas 2017 models on storm time conditions which occurred on 2015-06-23 as observed over KRTV station. Figures 14a–14c and Figures 14d–14f show patterns of the modelled VTEC and GPS-VTEC values when the storm option is “off” and “on”, respectively.

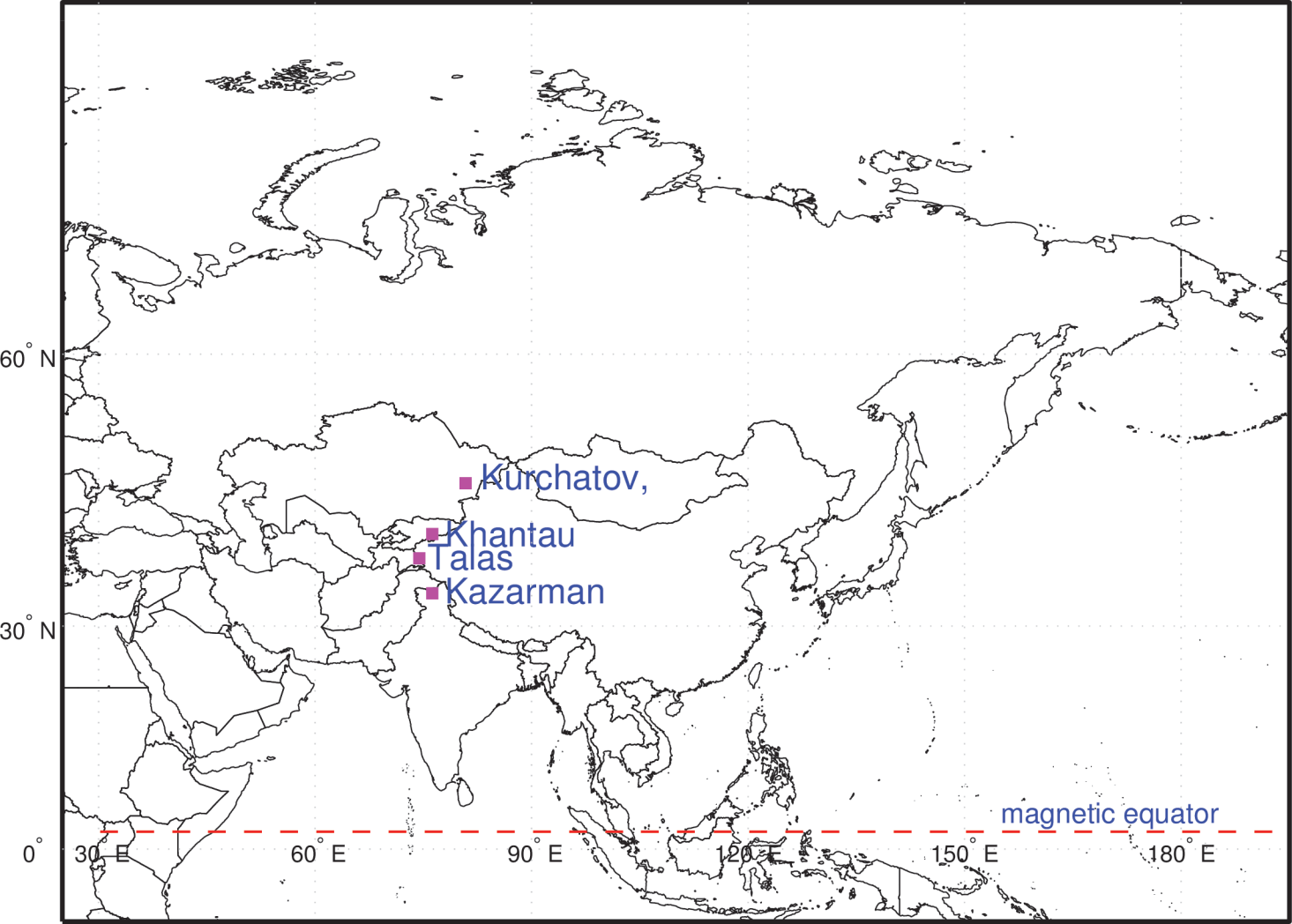
Kurchatov,
Khantau
Talas
Kazarman
magnetic equator
60° N
30° N
0°
30° E
60° E
90° E
120° E
150° E
180° E

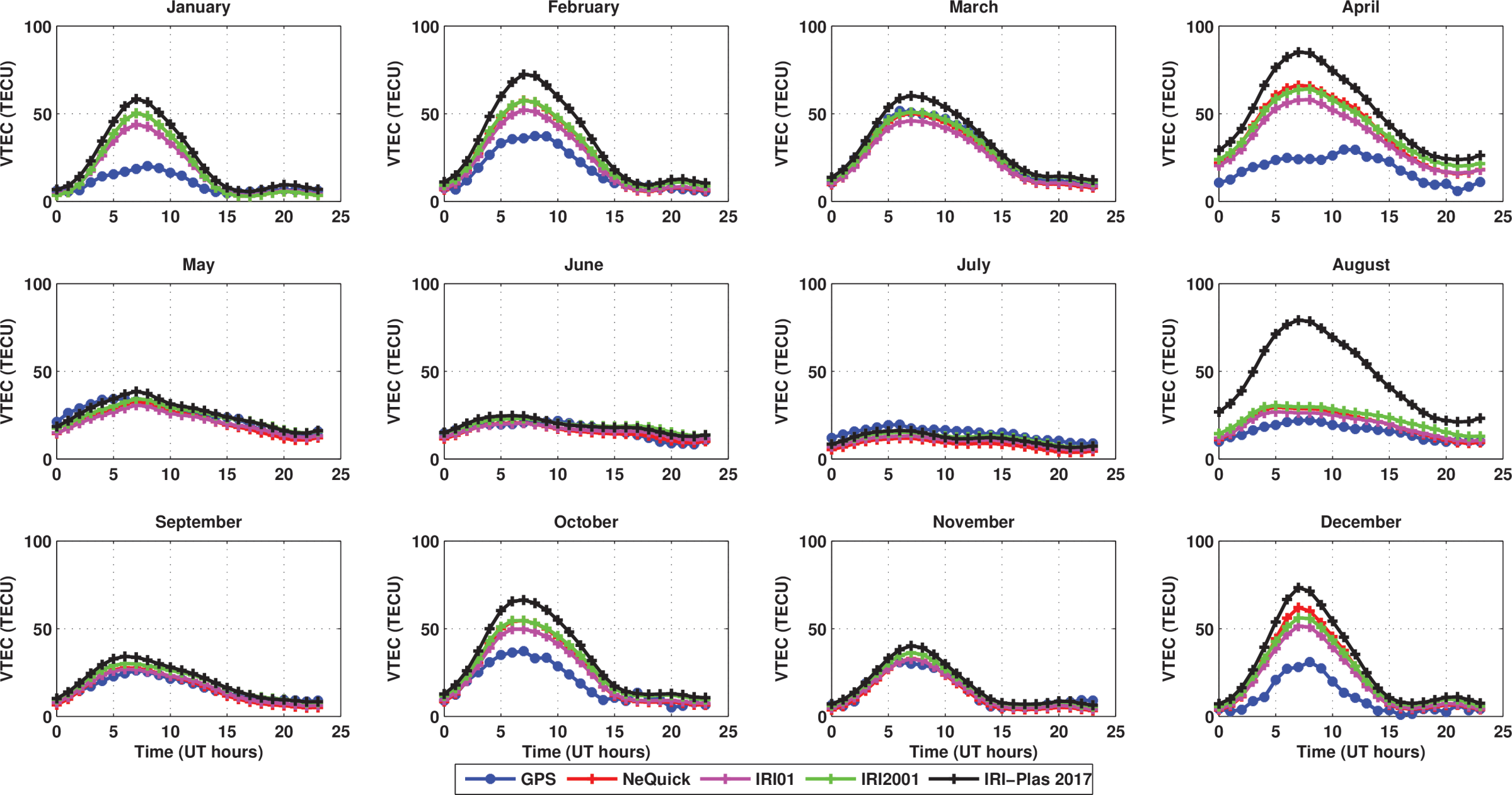
January
February
March
April
May
June
July
August
September
October
November
December
VTEC (TECU)
Time (UT hours)
0
50
100
0
5
10
15
20
25
GPS
NeQuick
IRI01
IRI2001
IRI–Plas 2017

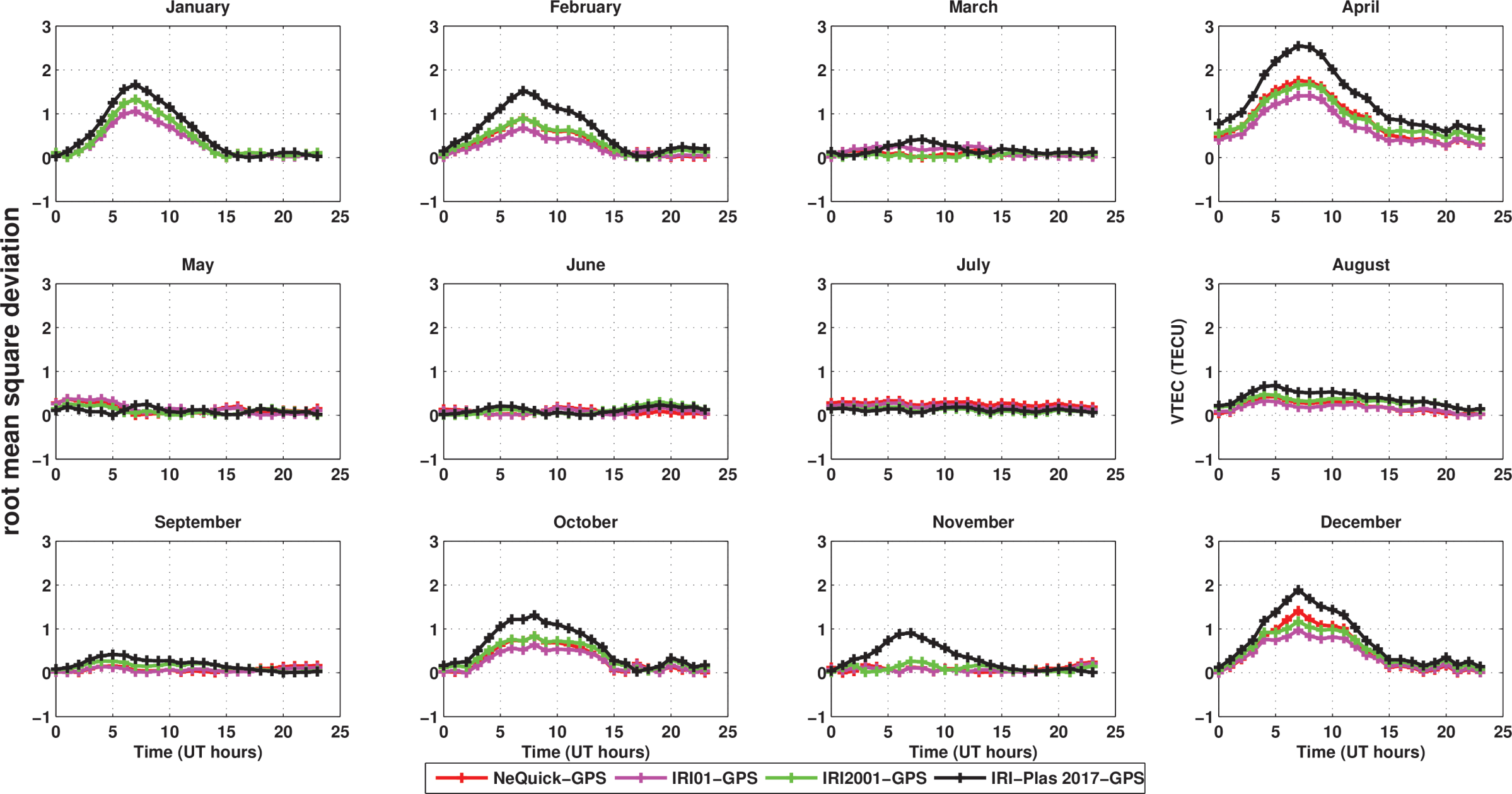
January
February
March
April
May
June
July
August
September
October
November
December
root mean square deviation
VTEC (TECU)
Time (UT hours)
NeQuick–GPS
IRI01–GPS
IRI2001–GPS
IRI–Plas 2017–GPS

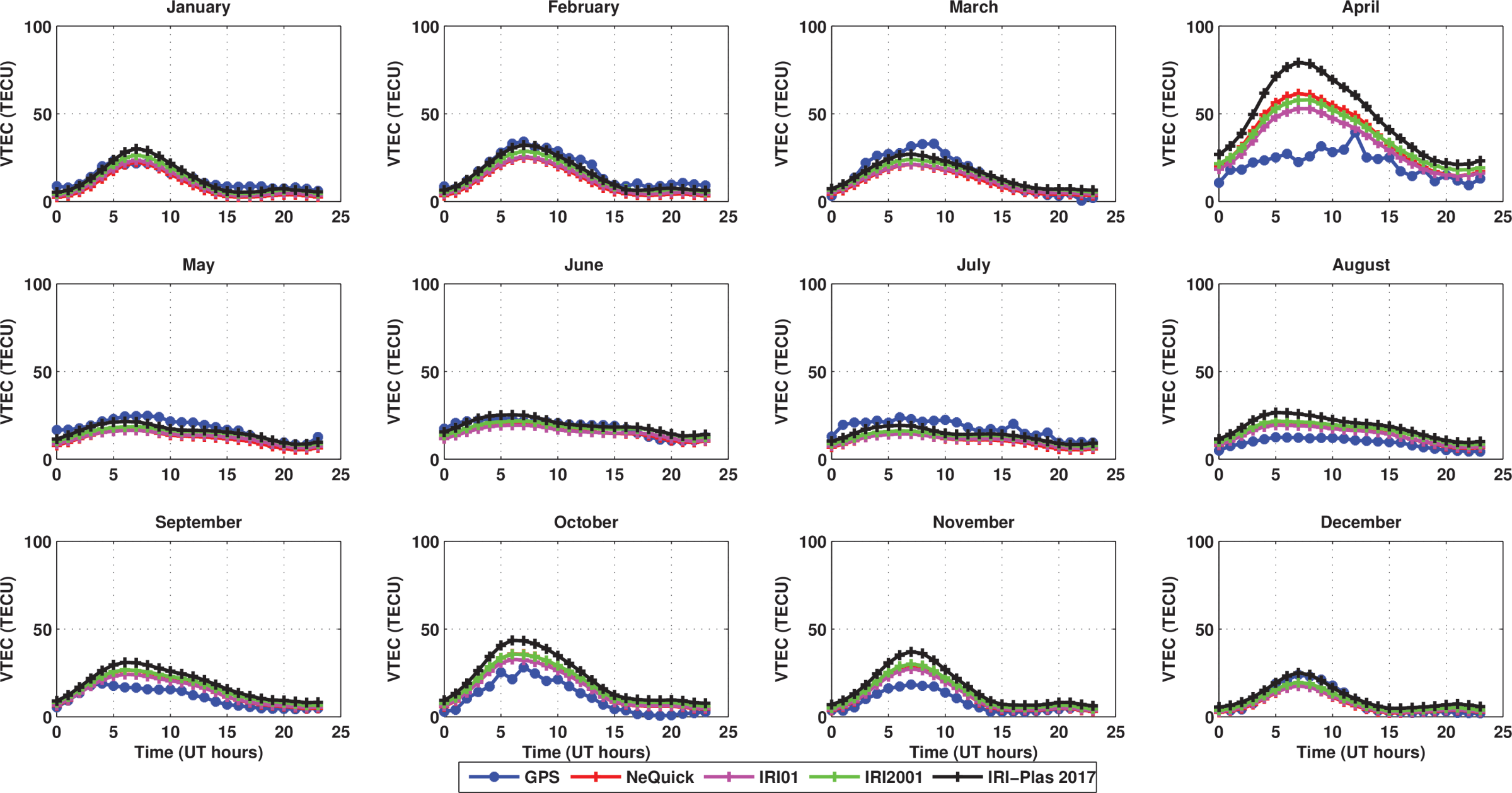
January
February
March
April
May
June
July
August
September
October
November
December
VTEC (TECU)
Time (UT hours)
0
50
100
0
5
10
15
20
25
GPS
NeQuick
IRI01
IRI2001
IRI-Plas 2017

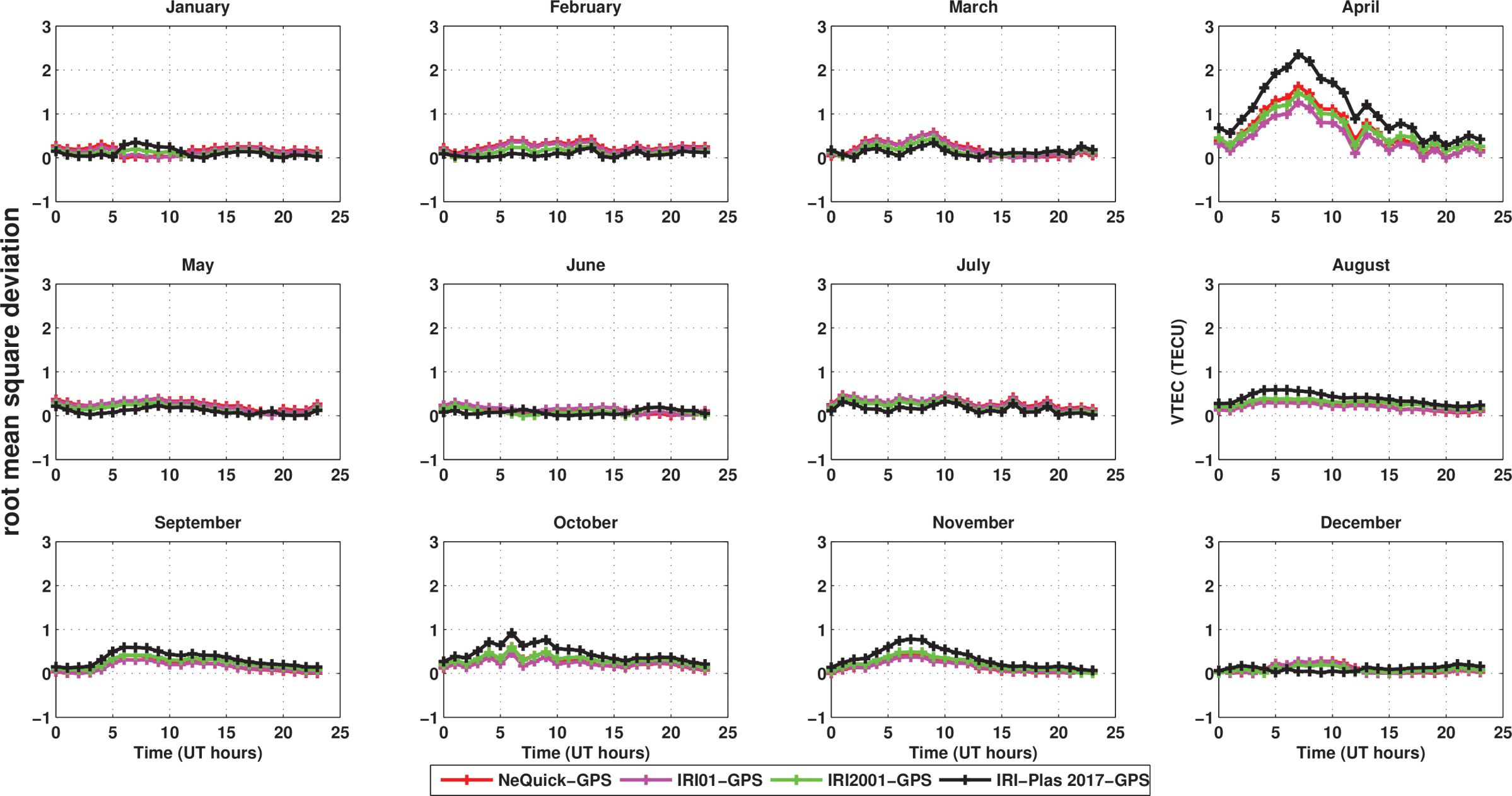
January
February
March
April
May
June
July
August
September
October
November
December
root mean square deviation
VTEC (TECU)
Time (UT hours)
NeQuick–GPS
IRI01–GPS
IRI2001–GPS
IRI–Plas 2017–GPS

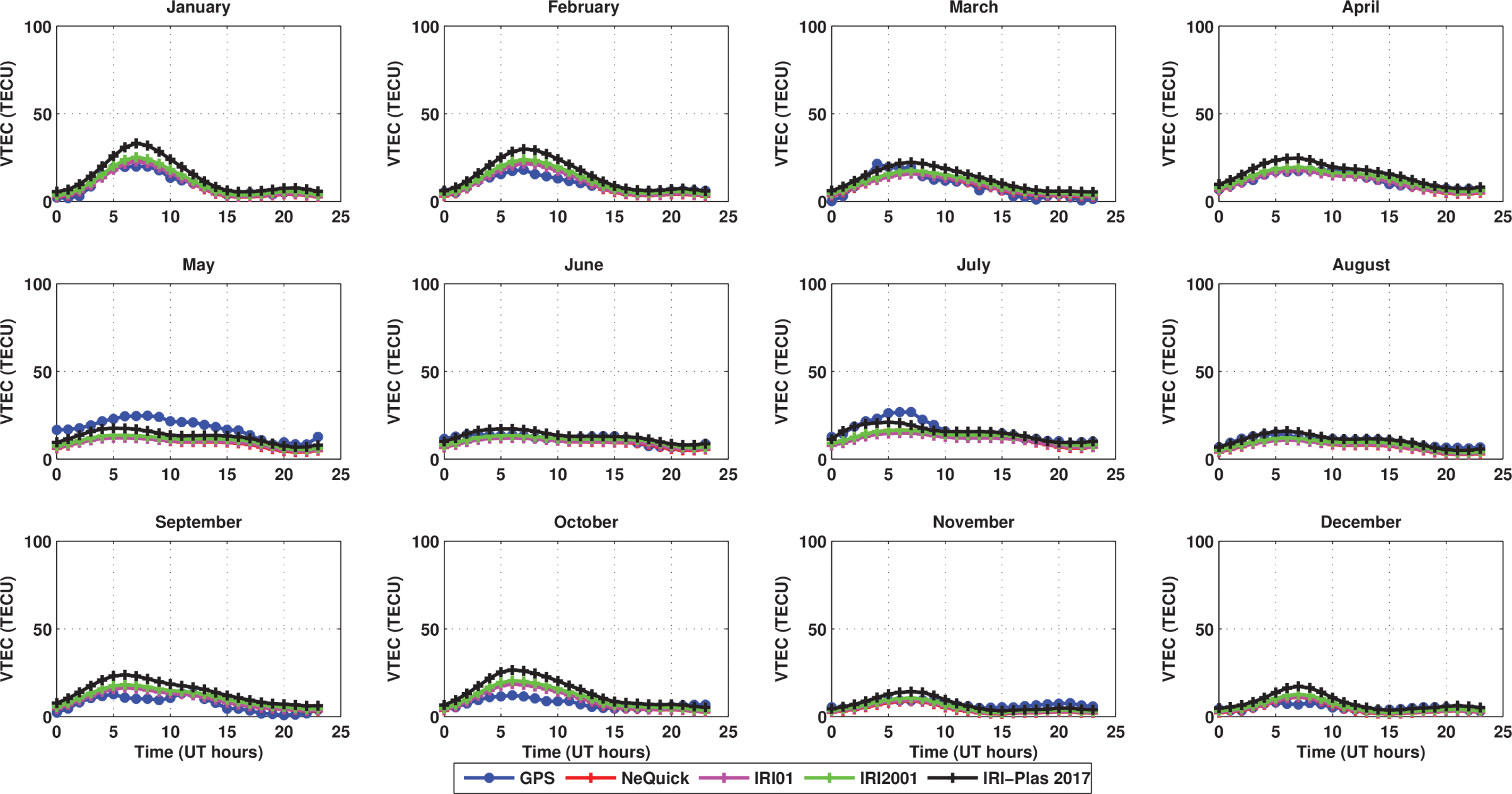
January
February
March
April
May
June
July
August
September
October
November
December
VTEC (TECU)
Time (UT hours)
0
50
100
0
5
10
15
20
25
GPS
NeQuick
IRI01
IRI2001
IRI–Plas 2017

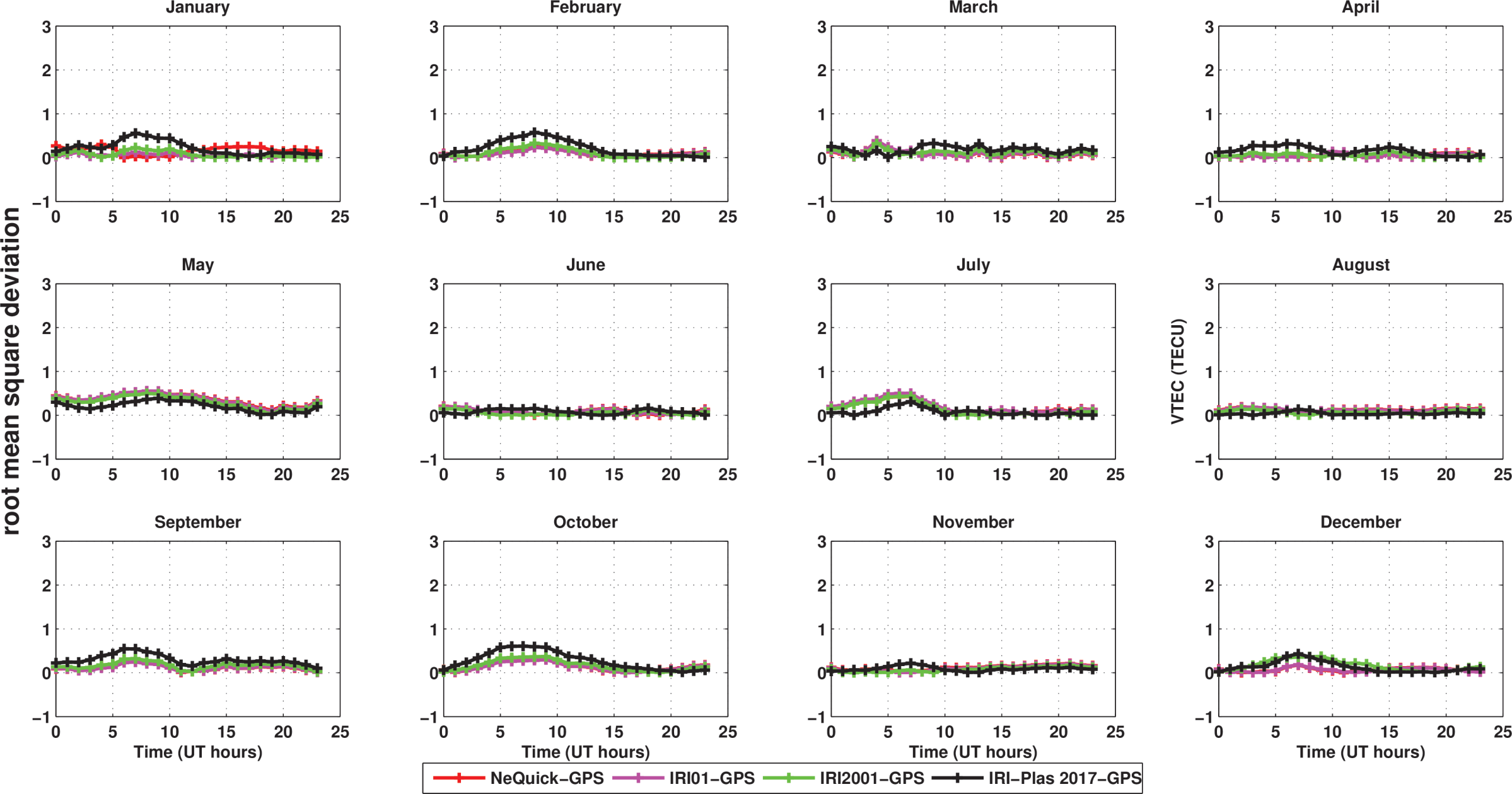
January
February
March
April
May
June
July
August
September
October
November
December
root mean square deviation
VTEC (TECU)
Time (UT hours)
NeQuick–GPS
IRI01–GPS
IRI2001–GPS
IRI–Plas 2017–GPS

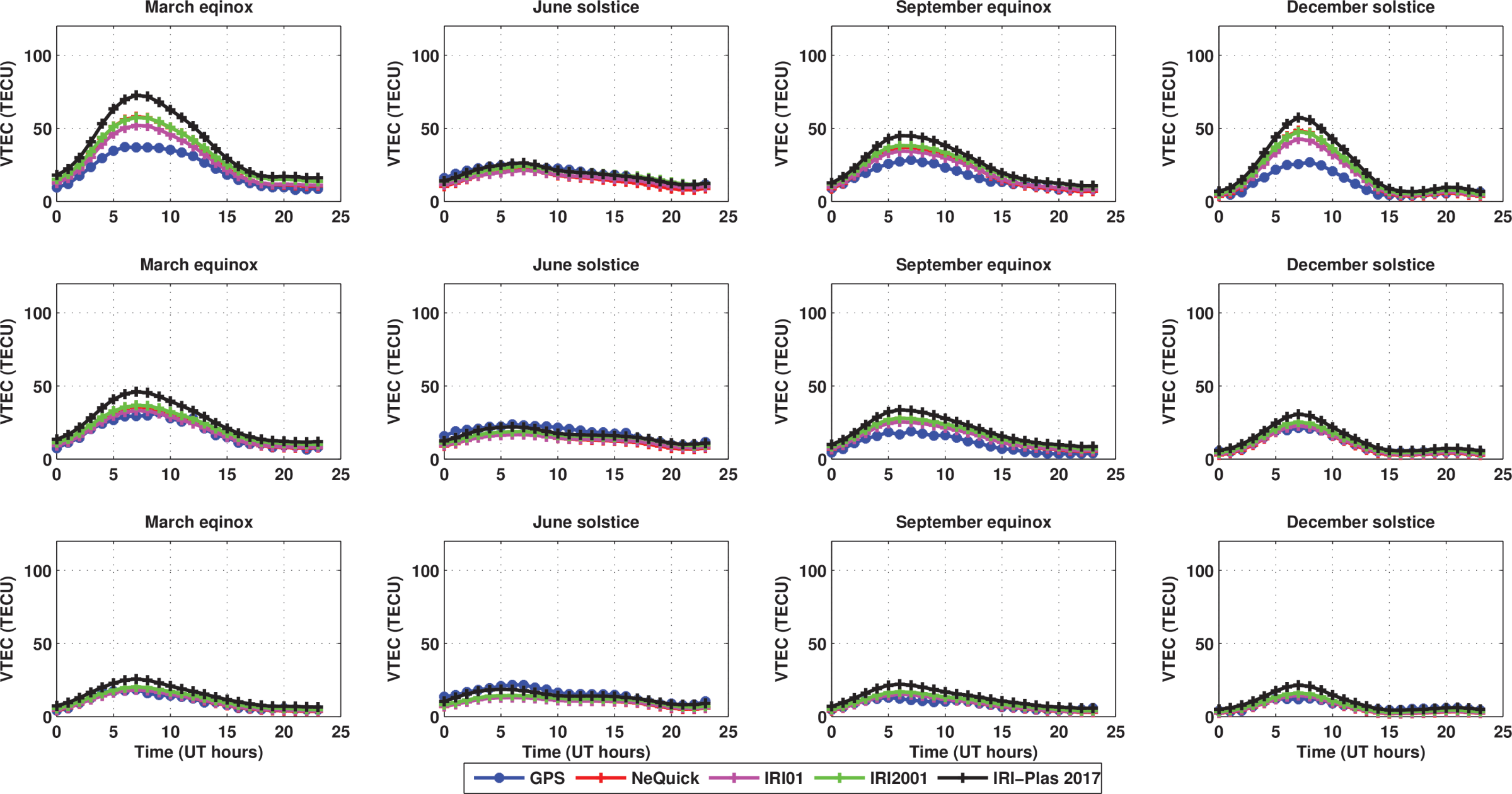
March eqinox
June solstice
September equinox
December solstice
March equinox
June solstice
September equinox
December solstice
March eqinox
June solstice
September equinox
December solstice
VTEC (TECU)
Time (UT hours)
0
50
100
0
5
10
15
20
25
GPS
NeQuick
IRI01
IRI2001
IRI–Plas 2017

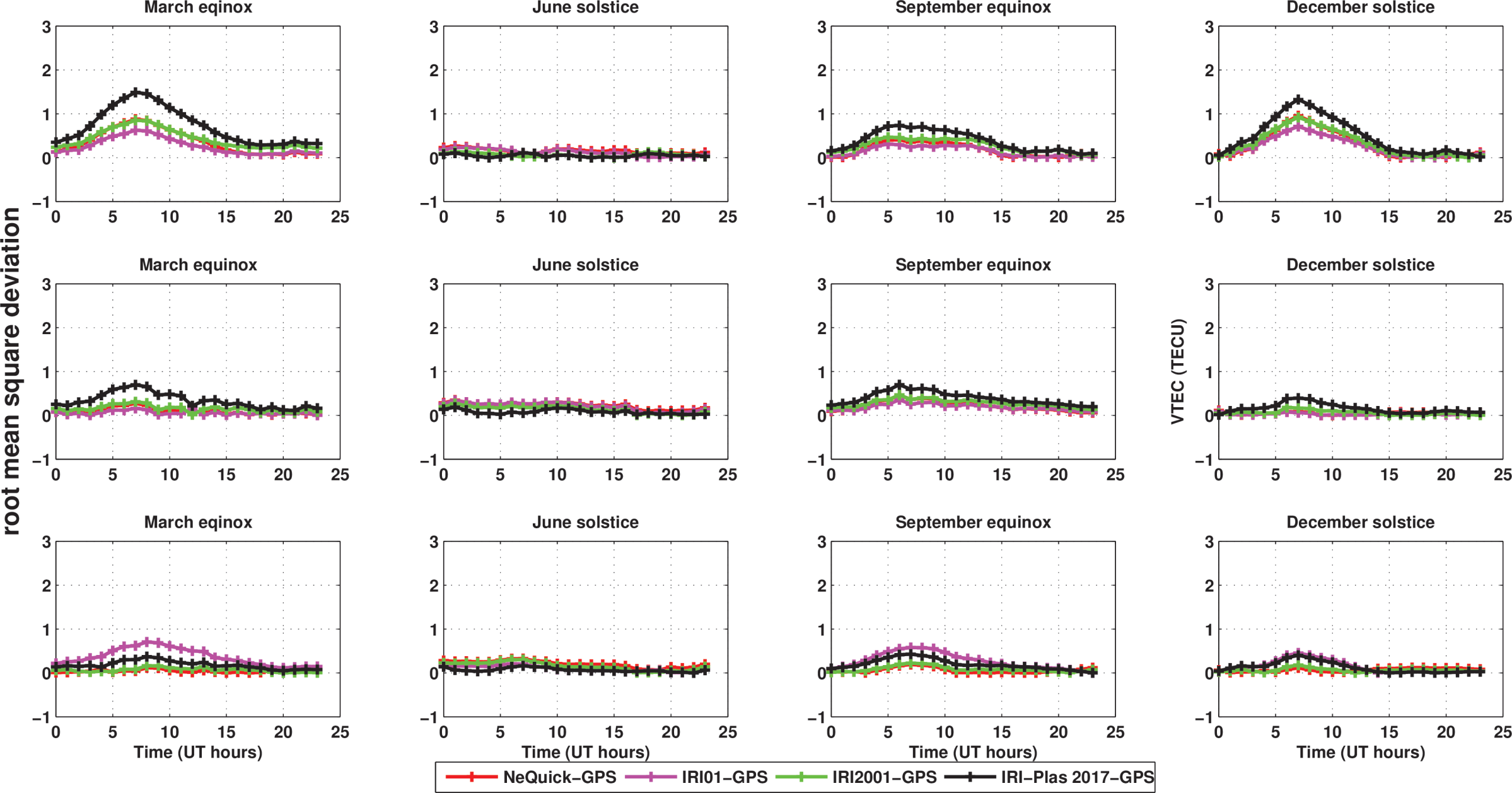
March eqinox
June solstice
September equinox
December solstice
March equinox
June solstice
September equinox
December solstice
March eqinox
June solstice
September equinox
December solstice
root mean square deviation
VTEC (TECU)
Time (UT hours)
Time (UT hours)
Time (UT hours)
Time (UT hours)
NeQuick−GPS
IRI01−GPS
IRI2001−GPS
IRI−Plas 2017−GPS

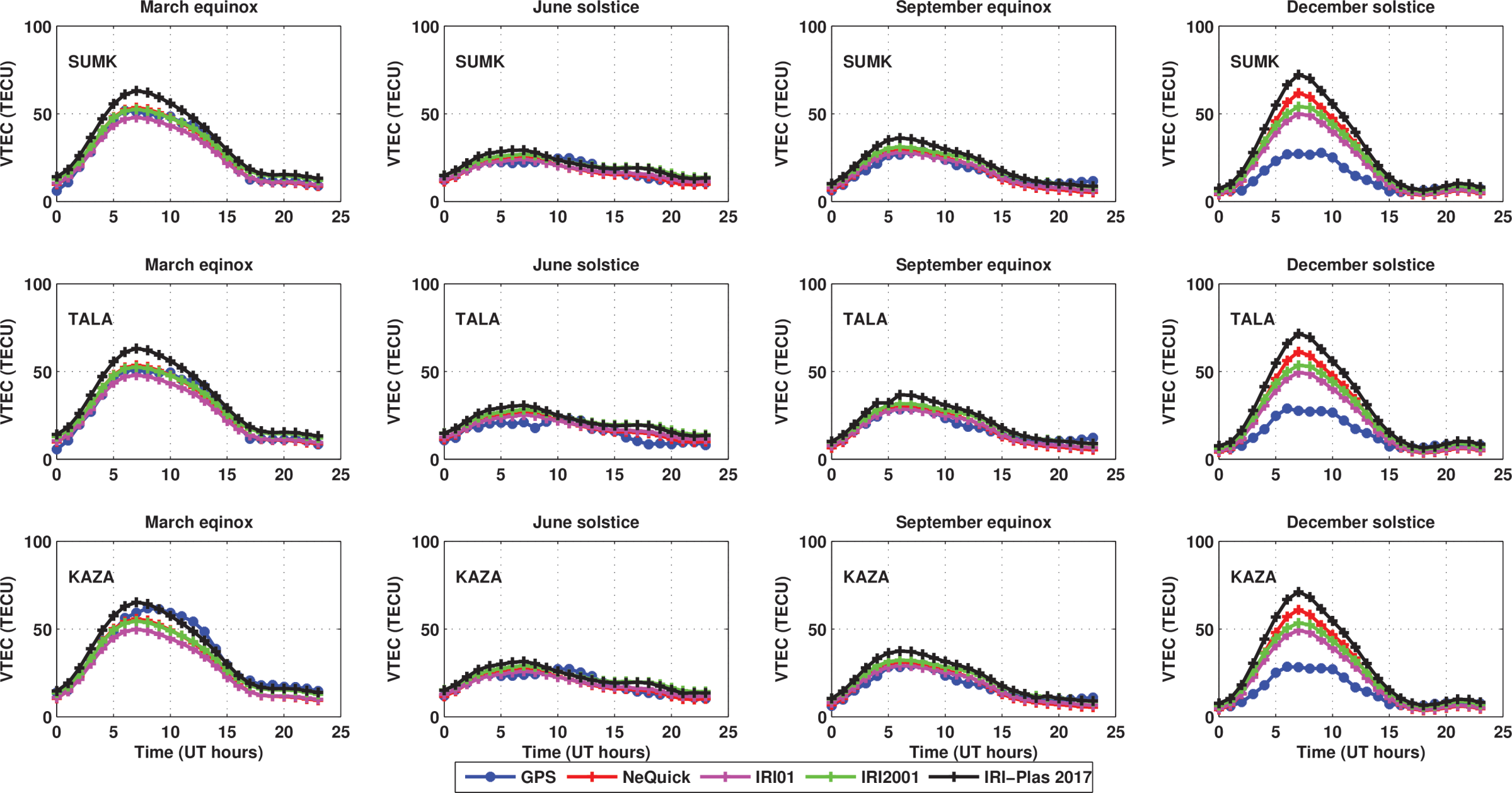
March equinox
June solstice
September equinox
December solstice
SUMK
TALA
KAZA
VTEC (TECU)
Time (UT hours)
GPS
NeQuick
IRI01
IRI2001
IRI–Plas 2017

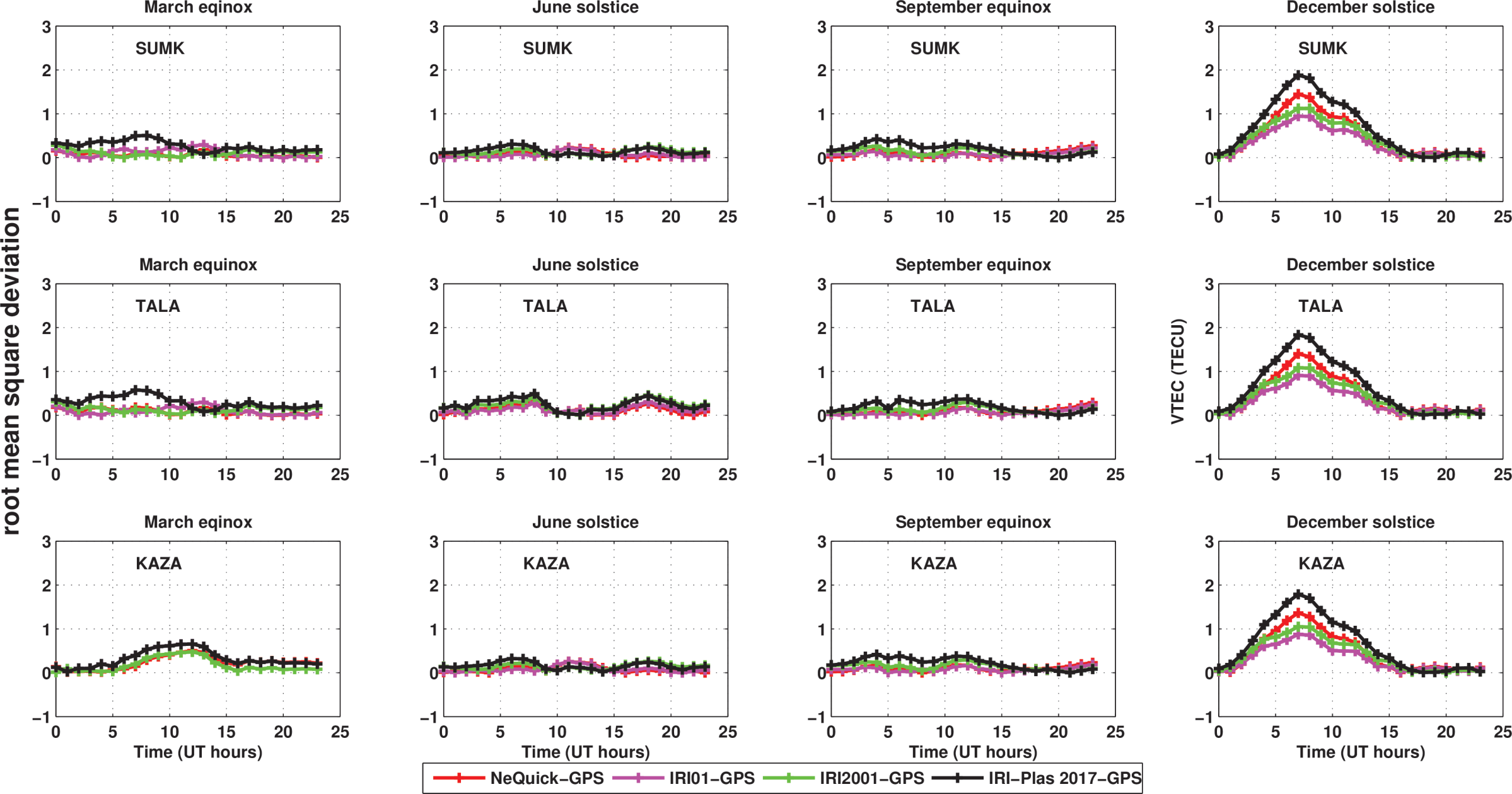
March eqinox
June solstice
September equinox
December solstice
SUMK
TALA
KAZA
root mean square deviation
VTEC (TECU)
Time (UT hours)
NeQuick–GPS
IRI01–GPS
IRI2001–GPS
IRI–Plas 2017–GPS

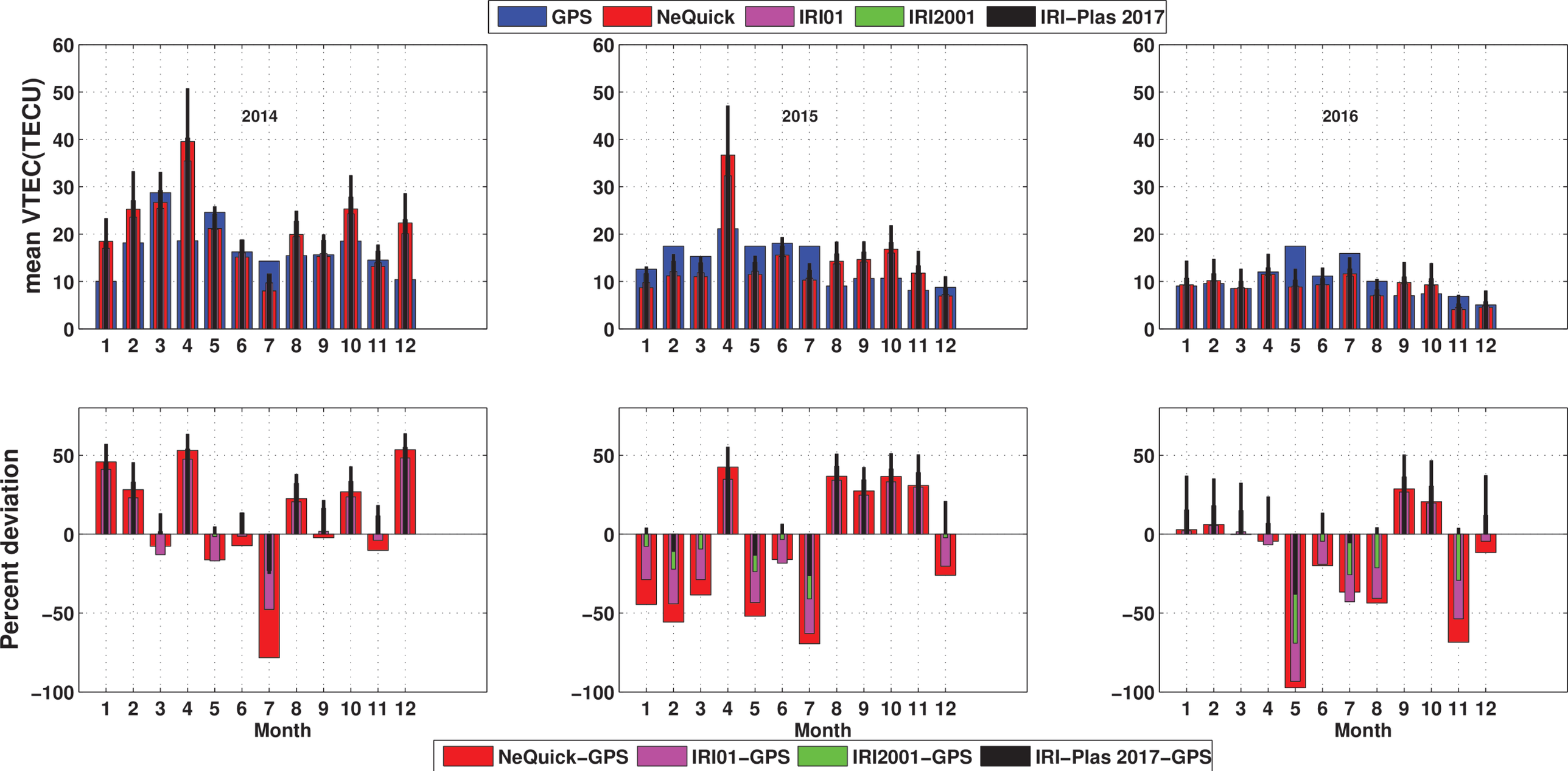
GPS
NeQuick
IRI01
IRI2001
IRI−Plas 2017
mean VTEC(TECU)
2014
2015
2016
Percent deviation
Month
NeQuick−GPS
IRI01−GPS
IRI2001−GPS
IRI−Plas 2017−GPS

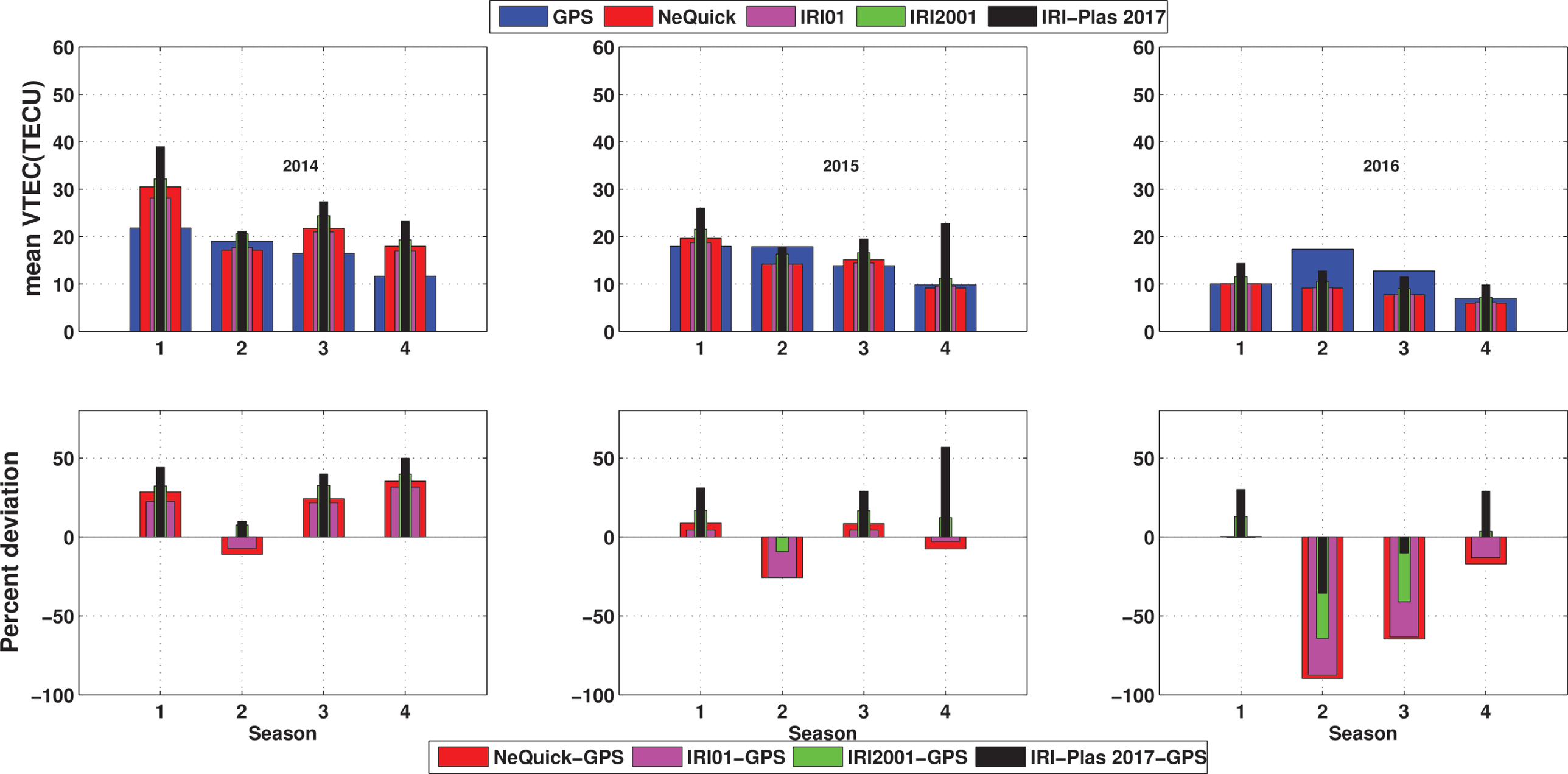
GPS
NeQuick
IRI01
IRI2001
IRI–Plas 2017
mean VTEC(TECU)
2014
2015
2016
Percent deviation
Season
NeQuick–GPS
IRI01–GPS
IRI2001–GPS
IRI–Plas 2017–GPS

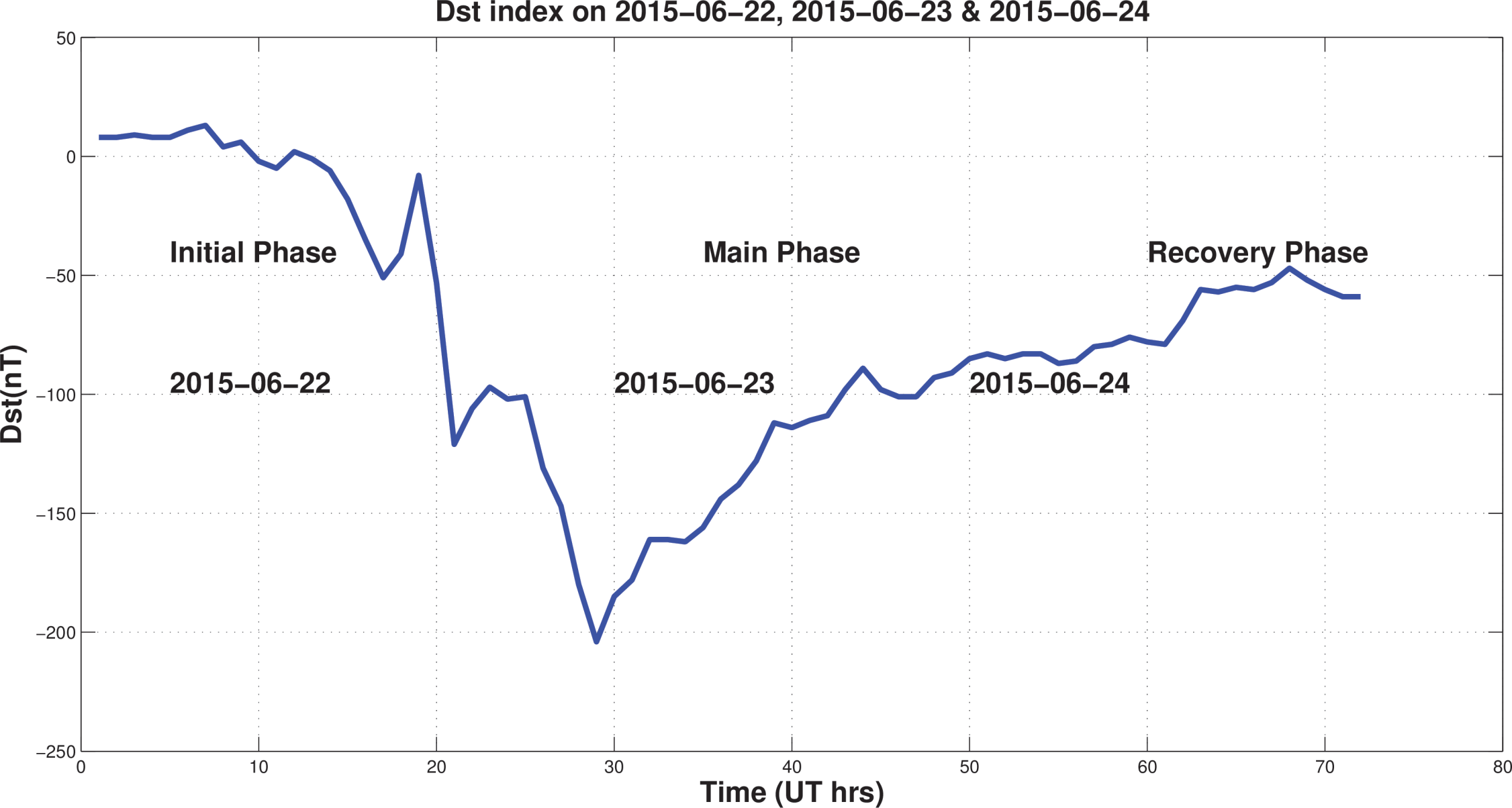
Dst index on 2015–06–22, 2015–06–23 & 2015–06–24
Initial Phase
Main Phase
Recovery Phase
2015–06–22
2015–06–23
2015–06–24
Dst(nT)
Time (UT hrs)
50
0
−50
−100
−150
−200
−250
0
10
20
30
40
50
60
70
80

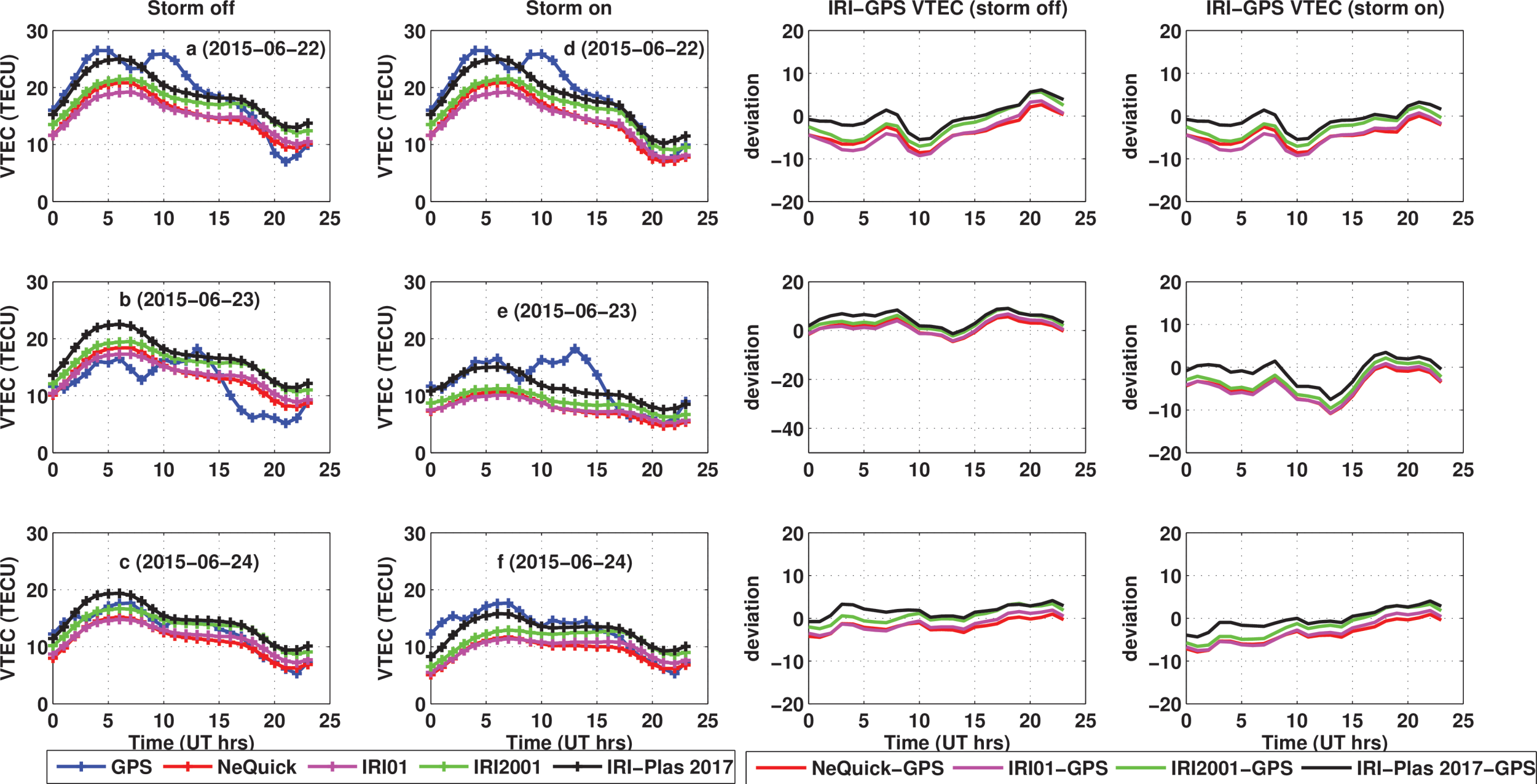
Storm off
Storm on
IRI–GPS VTEC (storm off)
IRI–GPS VTEC (storm on)
a (2015–06–22)
d (2015–06–22)
b (2015–06–23)
e (2015–06–23)
c (2015–06–24)
f (2015–06–24)
VTEC (TECU)
deviation
Time (UT hrs)
GPS
NeQuick
IRI01
IRI2001
IRI–Plas 2017
NeQuick–GPS
IRI01–GPS
IRI2001–GPS
IRI–Plas 2017–GPS